



**HAL**  
open science

## **Raman spectra analysis of ZrO<sub>2</sub> thermally grown on Zircaloy substrates irradiated with heavy ion: Effects of oxygen isotopic substitution**

Clément Ciszak, Michel Mermoux, Gaëlle Gutierrez, Frédéric Leprêtre, Christian Duriez, Ioana Popa, Laurent Fayette, Sébastien Chevalier

### ► To cite this version:

Clément Ciszak, Michel Mermoux, Gaëlle Gutierrez, Frédéric Leprêtre, Christian Duriez, et al.. Raman spectra analysis of ZrO<sub>2</sub> thermally grown on Zircaloy substrates irradiated with heavy ion: Effects of oxygen isotopic substitution. *Journal of Raman Spectroscopy*, 2019, 50 (3), pp.425-435. 10.1002/jrs.5513 . hal-02105028

**HAL Id: hal-02105028**

**<https://hal.science/hal-02105028>**

Submitted on 12 Apr 2021

**HAL** is a multi-disciplinary open access archive for the deposit and dissemination of scientific research documents, whether they are published or not. The documents may come from teaching and research institutions in France or abroad, or from public or private research centers.

L'archive ouverte pluridisciplinaire **HAL**, est destinée au dépôt et à la diffusion de documents scientifiques de niveau recherche, publiés ou non, émanant des établissements d'enseignement et de recherche français ou étrangers, des laboratoires publics ou privés.



OATAO is an open access repository that collects the work of Toulouse researchers and makes it freely available over the web where possible

This is an author's version published in: <http://oatao.univ-toulouse.fr/27628>

**Official URL:**


<https://doi.org/10.1002/jrs.5513>

**To cite this version:**

Ciszak, Clément and Mermoux, Michel and Gutierrez, Gaëlle and Leprêtre, Frédéric and Duriez, Christian and Popa, Ioana and Fayette, Laurent and Chevalier, Sébastien *Raman spectra analysis of ZrO<sub>2</sub> thermally grown on Zircaloy substrates irradiated with heavy ion: Effects of oxygen isotopic substitution.* (2019) *Journal of Raman Spectroscopy*, 50 (3). 425-435. ISSN 0377-0486

Any correspondence concerning this service should be sent to the repository administrator: [tech-oatao@listes-diff.inp-toulouse.fr](mailto:tech-oatao@listes-diff.inp-toulouse.fr)

# Raman spectra analysis of ZrO<sub>2</sub> thermally grown on Zircaloy substrates irradiated with heavy ion: Effects of oxygen isotopic substitution

Clément Ciszak<sup>1,2</sup>  | Michel Mermoux<sup>3</sup> | Gaëlle Gutierrez<sup>4</sup> | Frédéric Leprêtre<sup>4</sup> | Christian Duriez<sup>5</sup> | Ioana Popa<sup>2</sup> | Laurent Fayette<sup>1</sup> | Sébastien Chevalier<sup>2</sup>

<sup>1</sup> Commissariat à l'Énergie Atomique et aux Énergies Alternatives (CEA), DEN/DEC, Saint-Paul-lez-Durance, France

<sup>2</sup> ICB Laboratory, UMR 6303 CNRS, Univ. Bourgogne Franche-Comté, Dijon cedex, France

<sup>3</sup> CNRS, Grenoble INP, LEPMI, Univ. Grenoble Alpes, Univ. Savoie Mont Blanc, Grenoble, France

<sup>4</sup> Commissariat à l'Énergie Atomique et aux Énergies Alternatives (CEA), DEN/DANS/DMN, Gif-sur-Yvette, France

<sup>5</sup> Institut de Radioprotection et de Sécurité Nucléaire (IRSN), PSN-RES, Centre de Cadarache, Saint-Paul-lez-Durance, France

## Correspondence

Clément Ciszak, CIRIMAT-ENSIACET, UMR CNRS 5085, 31030 Toulouse, France.  
Email: clement.ciszak@ensiacet.fr

## Abstract

Recently, unusual Raman signals were observed in different works conducted on thin zirconia layers grown on zirconium alloys simulating in-reactor materials after high fluence ion irradiation or for samples cut from fuel rods irradiated in nuclear plants. As such, these spectra clearly do not correspond to any known spectrum of a pure standard zirconia phase. Therefore, the analysis conducted in this paper aims to provide a better understanding of these peculiar Raman features. For that purpose, specific ion-irradiated samples were analysed. *In situ* Raman spectroscopy was first used to follow the irradiation process. Then, samples were characterized using different excitation wavelengths. Finally, the effects of oxygen isotopic substitution were examined in details. Results are discussed in terms of disorder and size-related effects.

## KEYWORDS

<sup>18</sup>O labelling, ion irradiation, irradiation damage, Raman spectra, Zirconia

## 1 | INTRODUCTION

During in-pressurized water reactor operations, both inner and outer sides of the zirconium alloy cladding, enclosing the fuel pellets, are subjected to oxidation by the fuel for the inner one and by the primary coolant for the outer one. This leads to the progressive development of ZrO<sub>2</sub> layers that may exhibit a more or less complex structure depending on their growing environments and/or the origin of the corrosion processes, which obviously includes the nature of the irradiation phenomena affecting them.<sup>[1,2]</sup> Indeed, monoclinic zirconia, that is the thermodynamically stable phase at ambient pressure and temperature, is known to be sensitive to ion irradiation. As a matter of fact, induced damages may cause a partial or quasicomplete phase transition from monoclinic (m) to tetragonal (t) structure at sufficient

irradiation doses,<sup>[3–11]</sup> depending on the ion mass, energy, and fluence. This phase transition was usually evidenced with X-ray diffraction (XRD) measurements. As the discrimination between tetragonal and cubic (c) structures may be questionable from the XRD data, Raman spectroscopy is usually considered to be a simple and efficient alternative tool to follow this phase transition. However, this procedure may be much more complex than one simply expected because of the well-known strong difference of the characteristic spectra of the different zirconia polymorphs. Although the tetragonal phase in the irradiated commercial m-ZrO<sub>2</sub> powders or ceramics samples was recognized without any ambiguity from their corresponding Raman spectra,<sup>[3–7]</sup> unusual signals were recently observed on thin zirconia layers grown on zirconium alloys, simulating in-reactor materials after high fluence-ion irradiation<sup>[1,2,12–15]</sup> or even

for samples cuts from fuel rods irradiated up to an average burnup of  $58.7 \text{ GWd.tU}^{-1}$  in Gravelines 5 reactor (Electricité de France, France).<sup>[1,2]</sup> As described in the following, this peculiar Raman signature measured with 514 or 532 nm wavelengths is mostly composed by four apparent broad bands peaking approximately at about 185, 260, 615, and  $705 \text{ cm}^{-1}$ . In addition to these main bands, some smaller structures can also be seen. In the former case, partial XRD data tended to indicate a quasicomplete m-ZrO<sub>2</sub> to t-ZrO<sub>2</sub> phase transition, but these analyses were not systematically conducted. Moreover, comparing the different irradiation protocols used in previous studies,<sup>[1,2,12–15]</sup> it is difficult to extract a trend between the appearance of these unusual signals and the irradiation conditions; that is, the mass, energy, and fluence of the incident ions or particles. They were observed for light as well as heavy ion-irradiation (H, He, Au, Zr, Xe) for ion energies higher than 1 MeV and for fluences above  $10^{13}/\text{cm}^2$ . It seems that they were also partially observed for Ne irradiation at 150 Kev for fluences above  $10^{15}/\text{cm}^2$ .<sup>[15]</sup> For samples extracted from nuclear plants, these signals were exclusively observed close to metaloxide inner and outer interfaces, that is in regions *a priori* mainly subjected to neutron irradiation.<sup>[1,2]</sup> To our knowledge, only a few attempts were made to identify the origin of these peculiar signals.

Therefore, the analysis conducted in this paper aims to provide a better understanding of the nature and the modifications of these peculiar Raman features. Thus, complementary Raman measurements were performed using different excitation wavelengths on both virgin and ion-irradiated Zr<sup>16</sup>O<sub>2</sub> and labelled <sup>18</sup>O-enriched, thermally grown layers. Here, isotopic substitution was considered because it can bring different information.

First, isotope substitution is a unique tool for distinguishing different Raman active modes as it can lead to reliable mode assignments. This method provides a mass contrast: only vibrations involving the motion of the specific substituted atom will be shifted upon isotopic substitution. In the case of zirconia, the zone-centre Raman modes due to vibrations involving O atoms and those due to vibrations involving Zr atoms were successfully discerned using the Raman spectra of <sup>18</sup>O-labelled compounds.<sup>[16]</sup> This experimental assessment was further confirmed using *ab initio* calculations.<sup>[17]</sup> In addition, measurements of the zone-centre Raman wavenumbers for zirconia can be used as a versatile method to determine the isotopic concentration ratio with a fair accuracy.<sup>[18–20]</sup> This might be directly applied in two-stage oxidation experiments using isotopes as diffusion tracers, which are known in the corrosion community to give valuable inputs on diffusion processes.<sup>[21,22]</sup> For such a purpose, it has been demonstrated that <sup>18</sup>O concentration profiles or maps compare well with those that were

extracted from secondary ion mass spectroscopy analysis.<sup>[19,20]</sup> Finally, isotopic substitution can also be used to ascertain whether or not a given spectral structure is of vibrational origin or due to another type of excitation, for example, of electronic origin.

In this paper, following our previous report,<sup>[2]</sup> we focused on specific samples, thermally grown virgin and ion-irradiated Zr<sup>16</sup>O<sub>2</sub> and labelled, <sup>18</sup>O-enriched layers. Xe ions were selected as a compromise to simulate as best as possible the damage induced on zirconia by real fission recoils. Indeed, among the created fission products (FP) in nuclear fuel, Xe is one of the heaviest emitted fission recoils. Moreover, Xe is also commonly considered as the major gaseous FP, according to its relative abundance versus Kr (about 90% for 10% respectively). Xe was also selected to avoid any chemical interference between the incident ions and the target elements. It was shown that these irradiation conditions make it possible to reproduce the particular spectra observed for the spent fuel samples.<sup>[2]</sup>

These specific, labelled and unlabelled, virgin and ion-irradiated samples were described and analysed. *In situ* Raman spectroscopy was first used to follow the irradiation process. Then, samples were analysed using different excitation wavelengths. The results are tentatively discussed in terms of disorder, according to published zirconia total and partial vibrational density of states (VDOS). A particular attention has been paid to the effects of isotopic substitution.

## 2 | SAMPLES AND EXPERIMENTAL DETAILS

Samples were prepared from Zircaloy-4 discs (8 mm in diameter and about 1 mm thick) that were mechanically mirror polished prior to be oxidized in a thermobalance at 600 °C for 16 h in pure <sup>16</sup>O<sub>2</sub> and <sup>18</sup>O<sub>2</sub>-enriched atmospheres. It led in each case to the formation of a black, sub-stoichiometric, ZrO<sub>2</sub> layer. In the following, these samples are named Zr<sup>16</sup>O<sub>2</sub> and Zr<sup>18</sup>O<sub>2</sub>, respectively. In the last case, the <sup>18</sup>O average content in the layer was about 80%, as measured from mass spectrometry analysis of the gas phase used for the oxidation. The targeted zirconia scales thicknesses were in the 4–5 μm range, which has been further confirmed with optical microscopy. The two irradiated samples were then irradiated at room temperature with a 27 MeV Xe<sup>9+</sup> ion beam with flux of  $1 \times 10^{11} \text{ ion cm}^{-2} \text{ s}^{-1}$  up to a fluence of  $2.5 \times 10^{15} \text{ ion cm}^{-2}$ . The irradiations were performed at the Joint Accelerators for Nanoscience and Nuclear Simulation (JANNuS Saclay), CEA, France, on the EPIMETHEE accelerator. Using a specific cooling system, samples were maintained close to room temperature. The electronic and nuclear energy losses were calculated with the TRIM code,<sup>[1]</sup> and showed that the depth of the implanted Xe ions,

as expected, approximately corresponded to the film thicknesses, that is, approximately 4  $\mu\text{m}$ . After implantation, samples were cut for surface and cross-section examinations.

Reference monoclinic, yttrium-stabilized tetragonal and cubic zirconia samples were also available for comparison purposes.

The JANNuS facility, which also includes the possibility of *in situ* Raman monitoring during irradiation, was extensively described in the study of Miro et al. [13] Thus, Raman spectra were sequentially recorded during irradiation. The excitation wavelength was the 532 nm line of a Nd:YAG laser. Post irradiation analyses were performed using two different spectrometers. The first one was an InVia Renishaw spectrometer. This spectrometer was equipped with an air-cooled CCD detector, 2,400 and 1,200 grooves  $\text{mm}^{-1}$  gratings and a microscope. The excitation wavelength used were the 532 and 785 nm lines of a Nd:YAG and a diode laser, respectively. Spectra were acquired using 50 $\times$  and 100 $\times$  (NA = 0.75 and 0.9 respectively) objectives. Again, because unusual broad signals were observed, it was necessary to discriminate between Raman and photoluminescence signals. For such a purpose, we also used a Jobin-Yvon T64000 triple monochromator spectrometer and the 514, 488, and 325 nm excitation lines of Ar<sup>+</sup> ion and He-Cd laser, respectively. This spectrometer was equipped with a UV-enhanced liquid nitrogen-cooled CCD detector and a microscope. Spectra were acquired using a 50 $\times$  or a 40 $\times$  (NA = 0.75 and 0.5)

objective and 1,800 or 2,400 grooves  $\text{mm}^{-1}$  gratings in a subtractive configuration. Before each analysis, the output laser power was adjusted to avoid excessive heating of the sample. For this, the main criterion was to select a power density for which no evolution of the line shape of the spectra versus time was detectable. Indeed, the use of excessive incident power densities led to a fast and complete recovery of the m-ZrO<sub>2</sub> phase. [2] Within the exception of the UV excitation, typical acquisition times of individual spectra were in the 10–120 s range.

XRD measurements were performed at ICB laboratory with a Bruker D8 Advance diffractometer equipped with a LYNXEYE XE detector using Cu K $\alpha$  ( $\lambda = 0.154$  nm) radiation. The incidence angle has been varied in the 1–10 $^\circ$  range, to probe different thicknesses in the materials. Using such conditions, the calculated X-ray penetration depth was in the 400 nm – 4  $\mu\text{m}$  range.

### 3 | RESULTS

#### 3.1 | Particular effects of ion-irradiation on the Raman spectra of thermally grown ZrO<sub>2</sub> layers

Figure 1 describes the cross-section Raman profiles obtained on unirradiated Zr<sup>16</sup>O<sub>2</sub> (a) and Zr<sup>18</sup>O<sub>2</sub> (b) scales. The oxide layers were mostly composed of m-ZrO<sub>2</sub>, with a

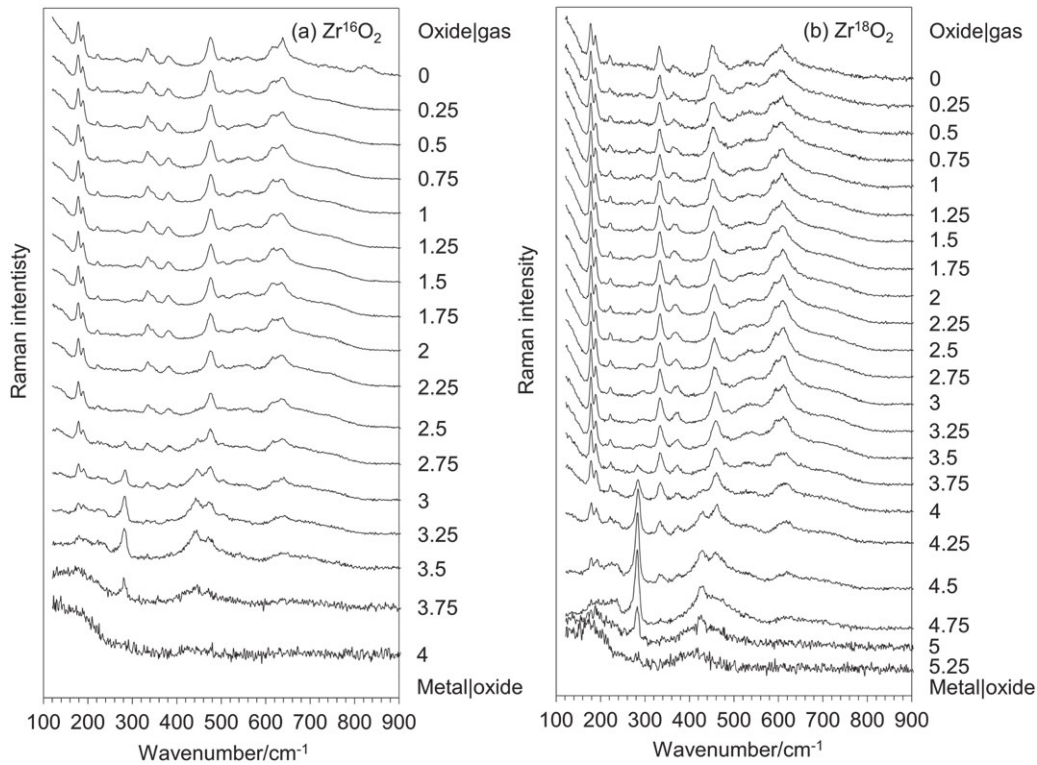


**FIGURE 1** Cross section Raman profiles obtained on unirradiated Zr<sup>16</sup>O<sub>2</sub> (a) and Zr<sup>18</sup>O<sub>2</sub> (b) scales. Corresponding positions are given in  $\mu\text{m}$  next to their respective spectrum. t-ZrO<sub>2</sub> is clearly identified close to the metaloxide interface, see the line at about 280  $\text{cm}^{-1}$

minor contribution of t-ZrO<sub>2</sub>, showing a good agreement with the literature.<sup>[23]</sup> As already observed, t-ZrO<sub>2</sub> was found to decorate the metaloxide interface with its own characteristic spectral features, in particular, a line at about 280 cm<sup>-1</sup>,<sup>[24,25]</sup> not further discussed in this paper. For the Zr<sup>18</sup>O<sub>2</sub> sample (Figure 1b), the line shifts of the high wavenumber m-ZrO<sub>2</sub> lines due to isotopic substitution corresponded to the expected ones.<sup>[16,18]</sup> That point will be discussed later.

As illustrated in Figure 2, several changes were observed on the Raman spectra after Xe<sup>9+</sup> ion beam irradiation. In that case, spectra were obtained with an excitation at 532 nm. For comparison purposes, a spectrum recorded for a spent fuel material, close to the inner metaloxide interface is also shown. It is seen that both spectra compare well. They systematically display broad and poorly resolved lines. This is a first strong indication of a high structural disorder and/or of materials with very small grains. For the spent fuel material, the aforementioned apparent four broad bands peaking at about 185,

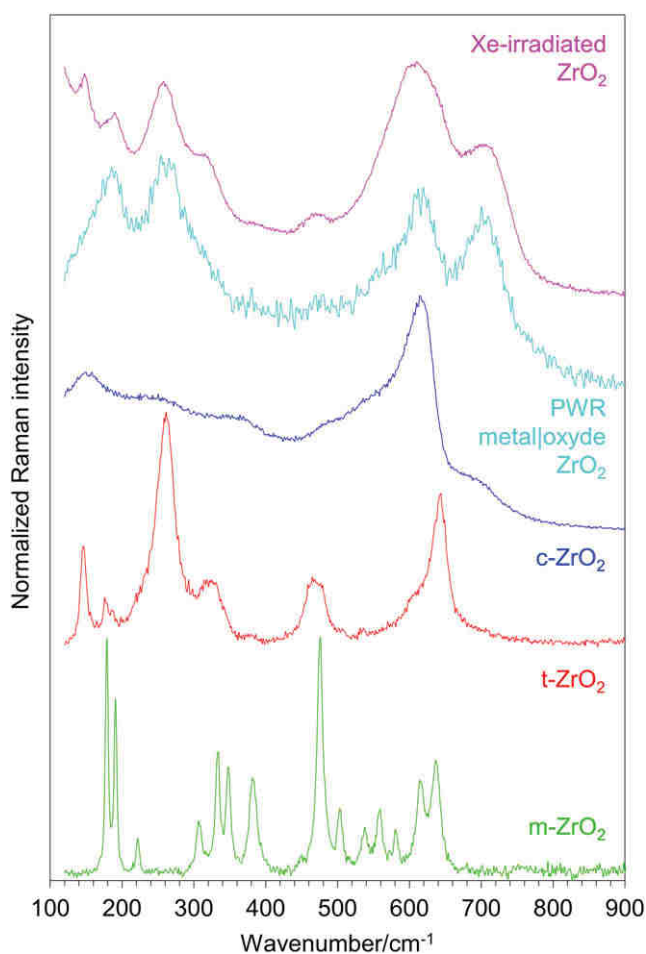


**FIGURE 2** Raman spectra of m-ZrO<sub>2</sub>, t-ZrO<sub>2</sub> (Y-stabilised), c-ZrO<sub>2</sub> (Y-stabilised) references, PWR metaloxide ZrO<sub>2</sub> from<sup>[1,2]</sup> and Xe-irradiated ZrO<sub>2</sub> [Colour figure can be viewed at [wileyonlinelibrary.com](http://wileyonlinelibrary.com)]

260, 615, and 705 cm<sup>-1</sup> were clearly observed, in spite of the low resolution of the spectrum that was obtained analyzing a highly radioactive material, in a hot cell.<sup>[1,2]</sup> The spectrum recorded for the “model” m-Zr<sup>16</sup>O<sub>2</sub> ion-irradiated material, of much higher quality, essentially reproduced the features observed for the spent fuel sample. In addition to these peaks, some smaller structures at 315 and 475 cm<sup>-1</sup> can also be seen, whereas line fitting procedures, always subjective in such a case, may suggest another apparent maxima, in particular at about 640 cm<sup>-1</sup>. Figure 2 also shows the well-known spectra of the different ZrO<sub>2</sub> polymorphs. Examination of the figure suggests that particular maxima are peaking close to some expected features, characteristic of ZrO<sub>2</sub> polymorphs. Thus, the first maximum around 185 cm<sup>-1</sup> may correspond to the low-wavenumber doublet of the m-ZrO<sub>2</sub> structure, the second one around 260 cm<sup>-1</sup> as well as the 315 cm<sup>-1</sup> shoulder to the t-ZrO<sub>2</sub> structure, and the third one at about 615 cm<sup>-1</sup> coincides with the expected most intense band of the c-ZrO<sub>2</sub> structure. However, although three lines, more or less, match the positions expected for m-ZrO<sub>2</sub> and t-ZrO<sub>2</sub>, or even c-ZrO<sub>2</sub>, as such, these spectra clearly do not correspond to any known spectrum of a pure standard zirconia phase.<sup>[1,2,12-15]</sup> In particular, the last broad line at about 705 cm<sup>-1</sup> does not correspond to any known zone-centre Raman mode of a zirconia polymorph. The spectrum recorded for the m-Zr<sup>18</sup>O<sub>2</sub> ion-irradiated material was similar in shape. Again, line shifts due to <sup>18</sup>O isotopic substitution will be discussed below.

*In situ* monitoring of the spectra evolution during irradiation gave additional information. As described in the experimental part, both zirconia scales were irradiated with a 27 MeV Xe<sup>9+</sup> ion beam on the EPIMETHEE accelerator, using a flux of  $1 \times 10^{11}$  ion cm<sup>-2</sup> s<sup>-1</sup> up to a fluence of  $2.5 \times 10^{15}$  ion cm<sup>-2</sup> at the JANNuS Saclay facility. Results obtained for the Zr<sup>16</sup>O<sub>2</sub> sample already described in the study of Ciszak et al.<sup>[2]</sup> are reported in Figure 3a for comparison. The results obtained on Zr<sup>18</sup>O<sub>2</sub> sample confirm the main trends, again within the exception of strong line shifts (Figure 3b). In both cases, the main evolution of the spectra is observed for fluences above  $\sim 10^{14}$ /cm<sup>2</sup>. This evolution first suggests a decrease of the m-ZrO<sub>2</sub> lines and an increase of some of the expected t-ZrO<sub>2</sub> lines. These intensity evolutions versus the irradiation dose follow a sigmoid-type law, as already observed from XRD data.<sup>[7]</sup> The diffraction pattern recorded after ion-irradiation with a 1° incidence angle clearly evidenced the presence of t-ZrO<sub>2</sub> with only a minor content of m-ZrO<sub>2</sub>: close to the sample surface, the phase transition is almost complete, see Figure S1. In agreement with all available data, no sign of amorphisation was detectable. As expected, before

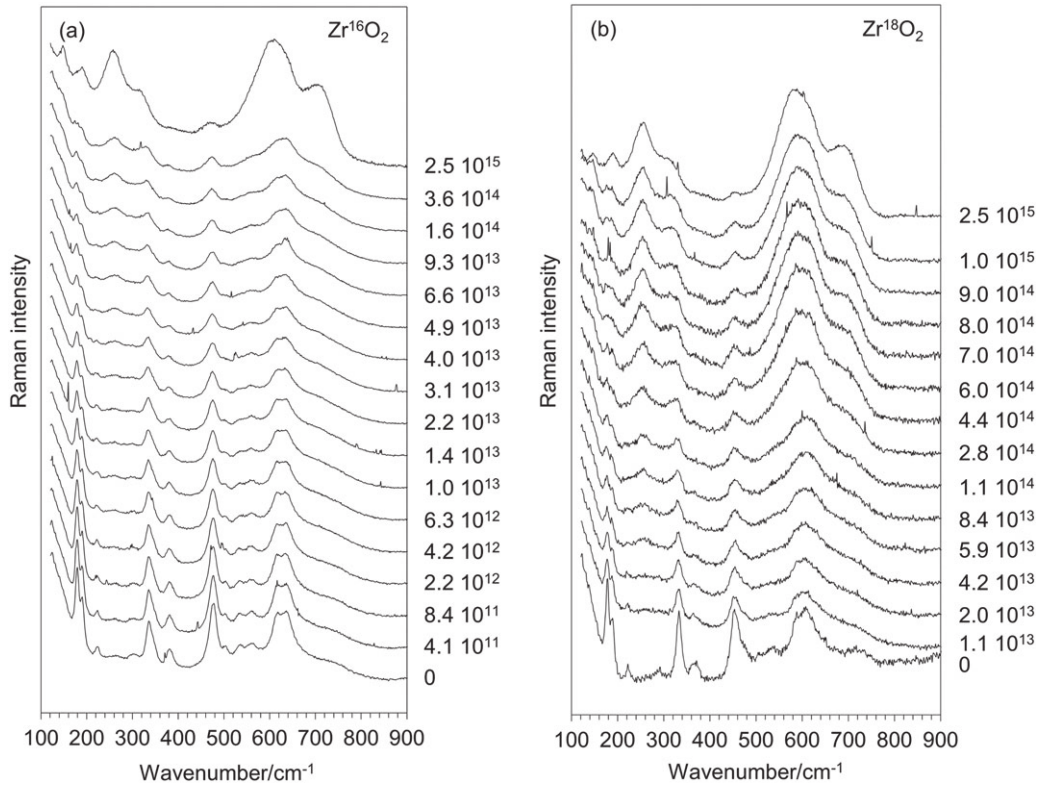


**FIGURE 3** *In situ* Raman monitoring of  $ZrO_2$  scales irradiated with 27 MeV  $Xe^{9+}$ . (a)  $Zr^{16}O_2$  scale from [1,2] (b)  $Zr^{18}O_2$  scale. Corresponding fluences are given in ion.  $cm^{-2}$  next to their respective spectrum. In both cases, a strong evolution of the spectra is observed for fluences above  $\sim 10^{14}/cm^2$

irradiation, the diffraction pattern was characteristic of the monoclinic phase, with a minor contribution of the tetragonal phase. This further suggests that the two maxima observed at low wavenumber (185 and 206  $cm^{-1}$ ) may be interpreted as being characteristic of m- $ZrO_2$  and t- $ZrO_2$  structures. On the other hand, this *in situ* monitoring did not give more insight on the two broad lines observed at higher wavenumbers (615 and 705  $cm^{-1}$ ). In particular, the presence of the c- $ZrO_2$  structure still cannot be excluded. From the figure, it is seen that both high wavenumber features tend to appear from the early beginning of the irradiation process and further gradually develop as the irradiation dose increases. Note also the high-relative intensity of the high wavenumber part of the spectra, which is not usually seen in the t- $ZrO_2$  spectra.

Cross-sectional Raman analysis confirmed that this signal was more or less homogeneously seen throughout the thickness of the irradiated samples, even if slight variations were observable (Figure 4). First, a lower m- $ZrO_2$  content was found close to the sample surface, as judged from the intensity of the 185  $cm^{-1}$  broad line, whereas its maximum intensity was found from and beyond the calculated maximum penetration depth of the incident Xe ions at about 4  $\mu m$ . Diffraction patterns recorded for different incidence angles confirmed that trend, that is, a higher m- $ZrO_2$  content when the incidence angle was

increased from 1 to 10°, see Figure S2 and Figure S3. Second, slight variations of the line profile of the high wavenumber 615 and 705  $cm^{-1}$  lines were observed in the form of line shifts as well as line intensity ratio variations. More in details, for the  $Zr^{16}O_2$  sample, going from the metaloxide interface up to the surface, there is a small upshift of the 705  $cm^{-1}$  and a small downshift of the 615  $cm^{-1}$  line. Deeper in the layer, a shoulder at about 570  $cm^{-1}$  is now clearly observable. In that last case, the shape of the signal between 500 and 650  $cm^{-1}$  overlaps almost perfectly with which is known for the c- $ZrO_2$ .

### 3.2 | Excitations at different wavelengths

To ascertain the origin of all the observed features, a first and necessary step was to exclude the presence of some possible photoluminescence lines in this wavenumber range. Thus, spectra were recorded using different excitation wavelengths, from 325 up to 785 nm. Main trends are summarized in Figure 5. First, the comparison of the spectra excited at 488, 514, and 532 nm and the absence of any significant signal in the 500–600 nm range when excited at 488 nm convincingly show that this particular signal was due to light scattering.<sup>[2]</sup> Second, there is a clear change in the line shape of the spectrum using an

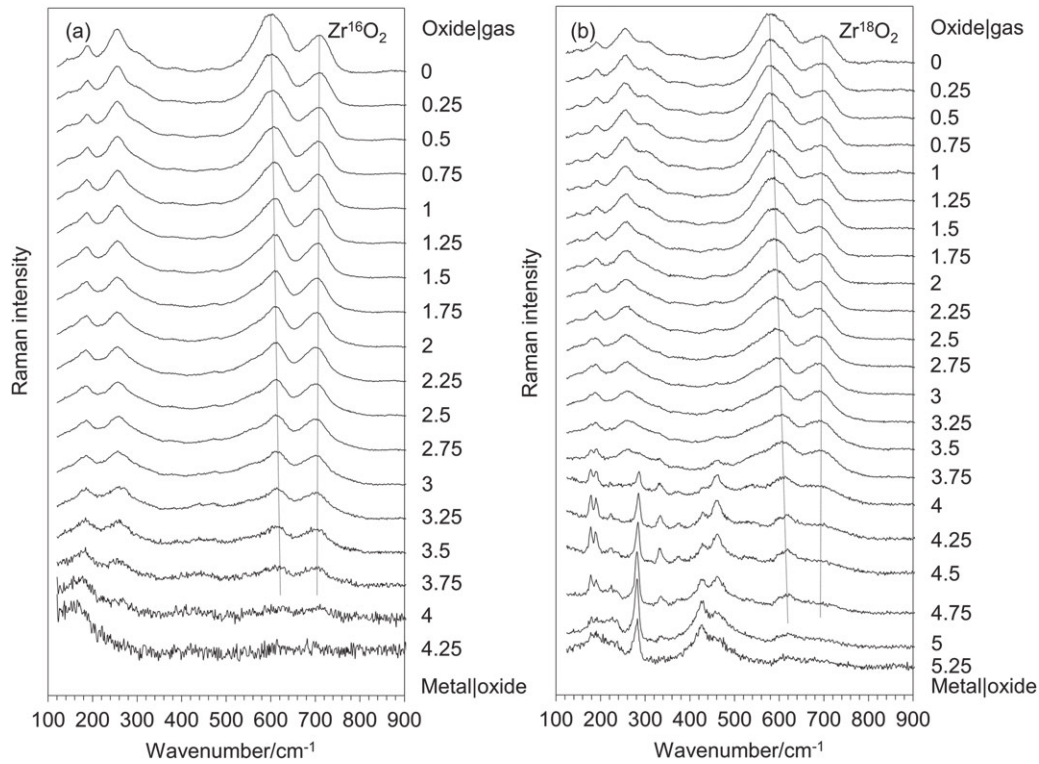


**FIGURE 4** Cross section Raman profiles obtained on Xe-irradiated  $Zr^{16}O_2$  (a) and  $Zr^{18}O_2$  (b) scales. Corresponding positions are given in  $\mu m$  next to their respective spectrum

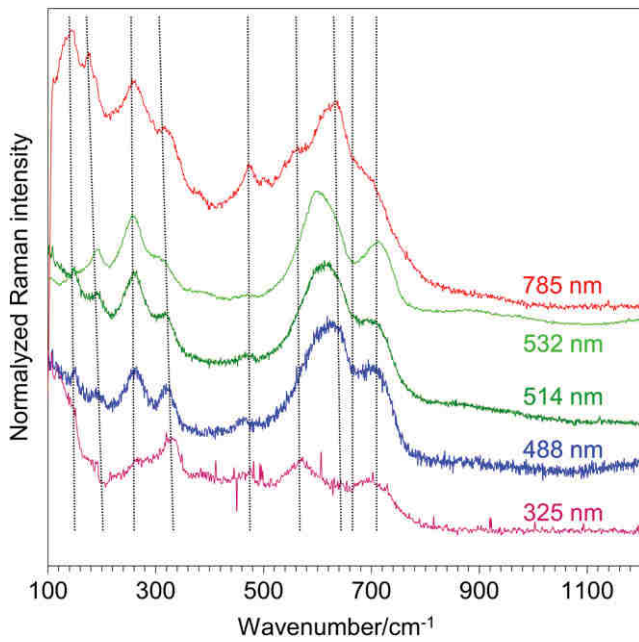


**FIGURE 5** Raman spectra of the Xe-irradiated  $Zr^{16}O_2$  layer obtained for excitation wavelengths of 325, 488, 514, 532, and 785 nm (from bottom to top) [Colour figure can be viewed at [wileyonlinelibrary.com](http://wileyonlinelibrary.com)]

excitation wavelength at 785 nm. In this last case, the spectrum was closer to the usual characteristics of t- $ZrO_2$ , with a minor contribution of m- $ZrO_2$ , in agreement with the diffraction data. Again, a strong broadening of the

main residual m- $ZrO_2$  and t- $ZrO_2$  lines, up twice as large as compared with a reference Y-doped t- $ZrO_2$  sample, reveals the disorder induced by the irradiation process. Furthermore, from the line shape of this particular spectrum, that is, the apparent maximum at about  $615\text{ cm}^{-1}$  and a clear shoulder at about  $560\text{ cm}^{-1}$ , the presence of c- $ZrO_2$  cannot be excluded. We give for information an example of spectrum obtained at 325 nm. This spectrum was very difficult to get, requiring very long acquisition times, up to 3,600 s. On the contrary, UV-excited spectra were readily obtained for the standard reference m- $ZrO_2$ , t- $ZrO_2$ , and c- $ZrO_2$  samples within short acquisition times. In all cases, these spectra exhibited their expected characteristics. First, this is an indication of a strong optical absorption of the irradiated materials at the analysis wavelength, which also means that the UV excitation leads to a near-surface analysis. This reflects a strong modification of the electronic properties of the irradiated- $ZrO_2$ , normally little absorbent in this wavenumber range. Second, this lack of signal is also an indication of a strong structural disorder at the sample surface.

### 3.3 | Excitations at different power densities

Another information was extracted from the line shape evolution versus the excitation power density. Most probably



because the ion-irradiated zirconia layer strongly absorbs visible and UV wavelengths, an increase of the excitation power density immediately led to a strong local heating of the sample. Within the exception of the 785 nm excitation, most of the measurements showed that the irradiated samples were unstable upon heating; the m-ZrO<sub>2</sub> was systematically recovered between 300 and 500°C, with kinetics that depended of the power density, that is, of the local temperature reached in the focused laser spot. In these experiments, the temperature was evaluated from the shift of the low frequency monoclinic lines and was therefore only a first rough estimate of the true sample temperature.<sup>[2]</sup> This was also an unexpected result while the t-ZrO<sub>2</sub> stabilized either with aliovalent dopants or small grain size is perfectly stable upon heating in this temperature range. Thus, this specific phase transition is not driven by macroscopic thermodynamic law, but rather by short-range effects at the nanometric scales.

At this stage, it is difficult to comment in more details the evolution of spectra line shapes as a function of the excitation wavelength, which may be due to variation in probing depth and/or to particular resonant scattering events. However, the absence of a clear signal evolution when near-IR excitation are used, that is, lower sample heating, if any, is an argument in favor of a significant change in probing depths with the excitation wavelength.

### 3.4 | Effects of the isotopic substitution

Considering the potential effects of irradiation, even if XRD did not evidence a strong sample amorphization, disorder considerations or static deformations of the zirconia lattice may be invoked for the understanding of those peculiar Raman signals. The translational disorder introduced by vacancies and/or interstitials atoms generated by ion-irradiation may obviously lead to a breakdown of selection rules. First, loss of translational order may allow symmetry-forbidden modes to be detected. Second, in the case of a strong disorder, the reduced Raman spectra ultimately represent the frequency distribution of the phonon density of states (VDOS). In the present case, the observed broad signal has an apparent cut-off wavenumber at about 830 cm<sup>-1</sup>, which matches the cut-off frequencies of the m-ZrO<sub>2</sub>, t-ZrO<sub>2</sub>, and even c-ZrO<sub>2</sub> polymorphs calculated VDOS.<sup>[26-30]</sup> Thus, it is tempting to interpret these spectra in terms of disorder.

To get further answer elements, characteristic spectra of the Zr<sup>16</sup>O<sub>2</sub> and Zr<sup>18</sup>O<sub>2</sub> scales were compared before and after the irradiation process. As a matter of fact, phonon frequencies are directly affected by changes of the average mass of the whole crystal or its sub-lattices, in a way that is usually described using the virtual crystal approximation (VCA), which implies that the force

constants do not depend on isotopic mass. The VCA approximation is usually introduced for a crystal containing several isotopes in order to recover the translational invariance lifted by the isotopic disorder. Masses of these isotopes are simply replaced by their average weighted by their relative abundances. For a monoatomic lattice with atoms of an average mass  $\mu$  in the harmonic approximation, any of the phonon frequencies, and not only the zone-centre ones, simply depend on the inverse of the square root of the average mass  $\mu^{-\frac{1}{2}}$ , for all wavevectors  $q$ .<sup>[31]</sup> In a lattice with different elements in the primitive cell, each element acts differently on the VCA frequencies, and this simple relation *a priori* does not hold for binary compounds; for which the changes of the phonon frequencies and atomic displacements with the mass of the constituent atoms are specific to each phonon branch and wave vector  $q$ . In contrast to elemental crystals, the mass dependence becomes  $q$  dependent.<sup>[31]</sup> Instead of phonon frequencies and dispersions, for example, given by *ab initio* calculations, the displacement patterns, that is, the phonon eigenvectors, have received much less attention and are not generally known. Information about the corresponding phonon eigenvector can be obtained by measuring the phonon frequency shifts induced by the atom mass change if samples with different isotopic compositions are available.

Thus, as a rule, the frequency of each line is expected to vary as  $\mu_{eff}^{-\frac{1}{2}}$ , where  $\mu_{eff}$  is the effective mass of the vibration. Again, a precise result interpretation requires a complete normal coordinate analysis to determine the effective masses for each mode. However, for our purpose, it is sufficient to make rough estimates based on limiting cases referring to the partial VDOS available from the literature.<sup>[26-29]</sup> In these partial VDOS and for all ZrO<sub>2</sub> phases, the heavier metal-dominated modes lie in the low energy part of the VDOS, whereas the lighter oxygen atoms tend to dominate in the high energy part of the frequency spectrum, more or less schematically above  $\sim 400-450$  cm<sup>-1</sup>, slightly depending on the specific polymorph. Therefore, according to this first approximation, in the high wavenumber range the shift induced by isotopic substitution of the Raman lines characteristic of all ZrO<sub>2</sub> phases should be estimated according to

$$\frac{\omega(Zr^{18}O_2)}{\omega(Zr^{16}O_2)} \sim \sqrt{\frac{\mu(^{16}O)}{\mu(^{18}O)}}, \quad (1)$$

where  $\mu(^{16}O)$  and  $\mu(^{18}O)$  are the masses calculated in both samples using the actual atomic percentage of <sup>16</sup>O and <sup>18</sup>O in the samples and  $\omega(Zr^{16}O_2)$  and  $\omega(Zr^{18}O_2)$  the corresponding mode frequencies. Here, the 0.2% natural abundance of <sup>18</sup>O can be neglected.

As expected, this is what is first seen in Figure 6a, the line shift of the six  $\text{ZrO}_2$  zone center Raman modes above  $400\text{ cm}^{-1}$  shift towards low wavenumbers in amounts consistent with the square root of the mass ratio  $^{16}\text{O}$  to  $^{18}\text{O}$ , and consistently gave the  $^{18}\text{O}$  content of the gas phase used for the oxidation (around 80%).<sup>[16,18]</sup> The seventh mode at  $758\text{ cm}^{-1}$  is not clearly resolved here. In agreement with previous studies,<sup>[16,18]</sup> only four zone-centre modes, located at about 178, 191, 220, and  $333\text{ cm}^{-1}$ , are unaffected by isotopic substitution that are close to pure Zr vibrations. Here, the 532 nm excitation was used.

Moreover, it is very clear that there is a continuous background of the spectrum superimposed on the Raman lines in the  $400\text{--}830\text{ cm}^{-1}$  range, which also exhibits an apparent maximum above  $700\text{ cm}^{-1}$  (Figure 6a). This broad signal was already observed on zirconia thin layers thermally grown on zirconium alloys. It was attributed to a strong substoichiometry in the layers, due to the anionic growth process, which implies oxygen vacancy migration from the metaloxide interface to the film surface.<sup>[20]</sup> Thus, the  $400\text{--}900\text{ cm}^{-1}$  range in the spectrum was fitted to a  $\mu^{-1}$  law. As well as for zone-centre modes, the whole high-frequency part of the spectrum may be scaled with the mass law given in Equation 1: with the “mass correction” of the frequency scale, the two spectra are superimposed, see Figure S4. Again, the fit reasonably well agrees to estimate the  $^{18}\text{O}$  average content of sample around 80%. As more or less expected from the examination of the partial VDOS, this dependence on the isotopic composition confirmed the vibrational origin of the modes involved in this frequency range, mostly relevant to pure O vibrations.

After irradiation, the overall observation was quite similar (Figure 6b). The high-wavenumber part of the spectrum was found to depend on the isotopic

composition, and could be consistently scaled with a similar, O-dominated, mass law. However, the  $^{18}\text{O}$  content extracted from the fitting process gave a concentration significantly lower than that expected around 65% instead of 80%. Among other reasons, a small contribution from the Zr atoms motion may explain this discrepancy, even if the modes remain dominated by the motion of O atoms. Tuning the excitation wavelength to 785 nm confirmed this trend. Again, the high-frequency part of the spectrum was found to depend on the isotopic composition. Scaling the spectra also gave a value close to 65%.

Thus, isotopic substitution unambiguously reveals phononic contributions to the Raman spectrum; all the Raman contributions having wavenumber higher than  $400\text{ cm}^{-1}$  mainly correspond to O-related vibrations.

## 4 | DISCUSSION

As described throughout this paper, a peculiar Raman signature, mostly composed of four apparent broad signals peaking approximately at 185, 260, 615 and  $705\text{ cm}^{-1}$ , was observed for ion-irradiated zirconia layers thermally-grown on Zircaloy-4 substrates. A similar signature was observed for spent fuel materials, close to the inner and outer metaloxide interfaces.

The evolution of the spectra with the excitation wavelength and the effects of O isotopic substitution show unambiguously that the peculiar  $\text{ZrO}_2$  signals described here are of vibrational origin. As they were observed for various implanted elements, any chemical interference between incident ions and target atoms can be ruled out. Moreover, they were consistently observed for different zirconium alloys, Zircaloy-4 and M5.<sup>[12]</sup> This means

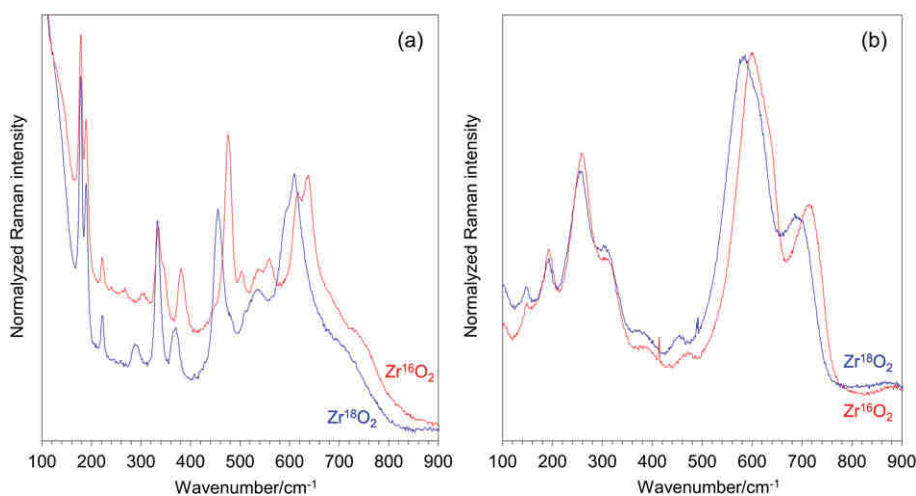


**FIGURE 6** Raman spectra of the virgin  $\text{Zr}^{16}\text{O}_2$  (red trace) and  $\text{Zr}^{18}\text{O}_2$  layers (blue trace) (a) and Xe-irradiated  $\text{Zr}^{16}\text{O}_2$  (red trace) and  $\text{Zr}^{18}\text{O}_2$  layers (blue trace) (b) [Colour figure can be viewed at [wileyonlinelibrary.com](http://wileyonlinelibrary.com)]

that the effect of the alloying elements is weak, if any. As a consequence of the irradiation process, we can discuss this particular signal in terms of structural disorder. XRD results help to precise the “location” of this structural disorder in terms of anionic and cationic sublattices. Indeed, in the case of  $\text{ZrO}_2$ , the high X-ray scattering factor of Zr versus O leads the diffraction pattern to be mainly representative of the Zr sublattice structure. Unlike Raman spectra, clear diffraction patterns were obtained before and after ion irradiation. Therefore, it is likely that the induced structural disorder mainly affects the O sublattice.

A first manifestation of such a disorder was a clear broadening of the observed Raman lines after the irradiation process. However, the *in situ* spectra evolution during the irradiation suggested that the first two broad bands at  $\sim 85$  and  $260 \text{ cm}^{-1}$  likely correspond to unresolved zone-centre, low frequency lines characteristic of m- $\text{ZrO}_2$  and t- $\text{ZrO}_2$ . The attribution of the third line is more uncertain insofar as it can correspond to broadened characteristic modes of the three polymorphs. The coexistence of the three  $\text{ZrO}_2$  polymorphs would explain the small variations of its profile during the analysis of the cross-sections. From the line shape of this particular line, the presence of c- $\text{ZrO}_2$  cannot be excluded.

The second manifestation of this disorder is the additional features appearance in the spectra, in particular above  $700 \text{ cm}^{-1}$ . This supplementary signal is partially seen before irradiation, but is clearly resolved at the end of the irradiation process. In this frequency range, the modes remain dominated by the motion of O atoms. At this point, two different interpretations may be offered.

On one hand, the observed additional features simply reflect a strong translational disorder in the O sublattice. It may be interpreted as disorder/defect-induced vibrational modes, normally symmetry-forbidden, which can become Raman active through a loss of symmetry because of a breakdown in the selection rules. This explanation may also hold, at least partially, for the  $615 \text{ cm}^{-1}$  broad line. A similar signal, observable as a shoulder, was identified for the layers before irradiation superimposed on the usual m- $\text{ZrO}_2$  characteristic Raman spectrum. For a further analysis of these signals, reference may be made to the calculated VDOS. Maxima in the  $600\text{--}710 \text{ cm}^{-1}$  range are effectively found in the calculated oxygen partial VDOS of both m- $\text{ZrO}_2$ , t- $\text{ZrO}_2$ , and even c- $\text{ZrO}_2$  at  $\sim 700$  and  $730 \text{ cm}^{-1}$  (m- $\text{ZrO}_2$ ),  $615$  and  $700 \text{ cm}^{-1}$  (t- $\text{ZrO}_2$ ), and  $640 \text{ cm}^{-1}$  (c- $\text{ZrO}_2$ ). Thus, if this hypothesis in terms of VDOS arguments is correct, the observation of this broad signal should reflect a strong disorder within the O sublattice, due to O vacancies in the case of the thermally grown scales or to ballistic

disorder in the case of the irradiated scales. Note that a similar shoulder at about  $700 \text{ cm}^{-1}$  is found on the Raman spectra of stabilized c- $\text{ZrO}_2$ , whereas its Raman spectrum is in part interpreted in terms of VDOS. In this last case, disorder in the O sublattice due to a high amount of O vacancies was also mentioned as the origin of such a broad signal.<sup>[32]</sup>

On the other hand, a model in which a substantial fraction of the O atoms are located in nonideal sites, giving rise to additional local vibrational modes cannot be excluded.

From our data, it is still not straightforward to explain the variability of the data available in the literature. In particular, this signal type has been seen on layers thermally grown on zirconium alloys and not on irradiated ceramics for which “conventional” t- $\text{ZrO}_2$  signals were unambiguously recorded after irradiation, without any clear indication of a strong disorder in their spectra. Up to now, bulk  $\text{ZrO}_2$  exhibited no evidence of irradiation-induced amorphization at very high doses. The material did not demonstrate a tendency towards amorphization, even in the most extreme irradiation conditions. However, at the smallest grain sizes, it was shown that radiation damage effects can be strongly enhanced.<sup>[33]</sup> In this paper, irradiation with  $1.0 \text{ MeV Xe}^{2+}$  ions of  $\sim 3 \text{ nm}$  diameter  $\text{ZrO}_2$  nanocrystals of tetragonal structure first led to a transition to the cubic structure and then to an amorphous state at the highest doses. Here, in the same way, it is perhaps possible to invoke the characteristic small grain size, in the  $10\text{--}50 \text{ nm}$  range of the thermally-grown oxidation layers, the presence of a high density of grain boundaries and their inherent substoichiometry,<sup>[23]</sup> which may amplify this disorder effect. At present, this size-related effect cannot be ruled out. This opens the way to many complementary studies, TEM measurements in particular.

## 5 | SUMMARY

A peculiar Raman signature mostly composed of four apparent broad signals peaking approximately at about  $185$ ,  $260$ ,  $615$ , and  $705 \text{ cm}^{-1}$  was observed for ion-irradiated zirconia layers thermally-grown on Zircaloy-4 substrates. A similar signature was observed for spent fuel materials close to the inner and outer metaloxide interfaces. To reproduce those Raman spectra, thermally grown zirconia layers were irradiated with a  $27 \text{ MeV Xe}^{9+}$  ion beam up to a fluence of  $2.5 \times 10^{15} \text{ ion cm}^{-2}$ . After irradiation, as already widely reported, XRD indicated a quasicomplete m- $\text{ZrO}_2$  to t- $\text{ZrO}_2$  phase transition. The evolution of the spectra with the excitation wavelength and the effects of O isotopic substitution show

unambiguously that the peculiar ZrO<sub>2</sub> signals described here are of vibrational origin. The first two broad bands at ~ 185 and 260 cm<sup>-1</sup> likely tracks the presence of m-ZrO<sub>2</sub> and t-ZrO<sub>2</sub>. From the line shape of the third band, the presence of c-ZrO<sub>2</sub> in the irradiated layers cannot be excluded. The last feature peaking at ~ 710 cm<sup>-1</sup> is likely a disorder/defect induced band, normally symmetry-forbidden, which can become Raman-active through a loss of symmetry due to the breakdown in the selection rules. This explanation may also hold, at least partially, for the 615 cm<sup>-1</sup> line. However, a model where a substantial fraction of the O atoms is located in nonideal sites, giving rise to additional local vibrational modes, cannot be excluded. To date, this peculiar signal seems to be essentially observed for oxidation layers, one of whose characteristics is their small grain size. Thus, we could suppose that this low grain size, along with the presence of a high density of grain boundaries and their inherent sub-stoichiometry, may amplify this disorder effect.

## ACKNOWLEDGEMENTS

EDF and Framatome are acknowledged for their technical and financial support. The authors would also like to thank Eric BORDAS for his technical support at the JANNuS Saclay facility. Likewise, the authors would like to thank Alexandre CRISCI (SIMAP, Grenoble, France) for technical support during some of the Raman experiments and special attention for this work.

## ORCID

Clément Ciszak  <http://orcid.org/0000-0003-4097-1015>

## REFERENCES

- [1] C. Ciszak, *Etude de l'accrochage pastille/gaine des crayons combustibles des réacteurs à eau pressurisée*, PhD, Université de Bourgogne Franche-Comté, Dijon, France **2017**.
- [2] C. Ciszak, M. Mermoux, S. Miro, G. Gutierrez, F. Lepretre, I. Popa, K. Hanifi, I. Zacharie-Aubrun, L. Fayette, S. Chevalier, *J. Nucl. Mater.* **2017**, 495, 392.
- [3] D. Simeone, J. L. Bechade, D. Gosset, A. Chevarier, P. Daniel, H. Pilliaire, G. Baldinozzi, *J. Nucl. Mater.* **2000**, 281, 171.
- [4] A. Benyagoub, F. Levesque, F. Couvreur, C. Gibert-Mougel, C. Dufour, E. Paumier, *Appl. Phys. Lett.* **2000**, 77, 3197.
- [5] J.-M. Costantini, A. Kahn-Harari, F. Beuneu, F. Couvreur, *J. Appl. Phys.* **2006**, 99, 123501.
- [6] B. Schuster, F. Fujara, B. Merk, R. Neumann, T. Seidl, C. Trautmann, *Nucl. Instrum. Methods Phys. Res. Sect. B beam interact. Mater. At.* **2012**, 277, 45.
- [7] C. Gibert-Mougel, F. Couvreur, J. M. Costantini, S. Bouffard, F. Levesque, S. Hémon, E. Paumier, C. Dufour, *J. Nucl. Mater.* **2001**, 295, 121.
- [8] D. Simeone, D. Gosset, J. L. Bechade, A. Chevarier, *J. Nucl. Mater.* **2002**, 300, 27.
- [9] D. Simeone, G. Baldinozzi, D. Gosset, S. LeCaër, L. Mazerolles, *Phys. Rev. B* **2004**, 70, 134116.
- [10] B. Schuster, M. Lang, R. Klein, C. Trautmann, R. Neumann, A. Benyagoub, *Nucl. Instrum. Methods Phys. Res. Sect. B beam interact. Mater. At.* **2009**, 267, 964.
- [11] A. Sharma, M. Varshney, H.-J. Shin, Y. Kumar, S. Gautam, K. H. Chae, *Chem. Phys. Lett.* **2014**, 592, 85.
- [12] R. Verlet, *Influence de l'irradiation et de la radiolyse sur la vitesse et les mécanismes de corrosion des alliages de zirconium*, PhD, EMSE, Saint-Etienne, France **2015**.
- [13] S. Miro, E. Bordas, L. Thomé, J.-M. Costantini, F. Leprêtre, P. Trocellier, Y. Serruys, L. Beck, D. Gosset, R. Verlet, J. Huguet-Garcia, M. Tupin, M. Belleil, *J. Raman Spectrosc.* **2016**, 47, 476.
- [14] R. Verlet, M. Tupin, G. Baldacchino, K. Wolski, S. Miro, D. Gosset, K. Colas, M. Jublot, F. Jomard, *Corros. Sci.* **2015**, 98, 327.
- [15] J. A. Valdez, Z. Chi, K. E. Sickafus, *J. Nucl. Mater.* **2008**, 381, 259.
- [16] B.-K. Kim, H. Hamaguchi, *Phys. Status Solidi B* **1997**, 203, 557.
- [17] D. A. Daramola, M. Muthuvel, G. G. Botte, *J. Phys. Chem. B* **2010**, 114, 9323.
- [18] M. Guérain, M. Mermoux, C. Duriez, *Corros. Sci.* **2015**, 98, 140.
- [19] A. Kasperski, M. Guérain, M. Mermoux, F. Jomard, *Oxid. Met.* **2017**, 87, 501.
- [20] A. Kasperski, C. Duriez, M. Mermoux, *Zircon. Nucl. Ind. 18th Int. Symp.* **2018**.
- [21] S. Chevalier, G. Strehl, J. Favergeon, F. Desserrey, S. Weber, O. Heintz, G. Borchardt, J. P. Larpin, *Mater. High Temp.* **2003**, 20, 253.
- [22] S. Chevalier, J. Favergeon (Eds), *French Activity on High Temperature Corrosion in Water Vapor*, Trans Tech Publ, Durnten-Zurich **2014**.
- [23] A. Motta, A. Yilmazbayhan, R. Comstock, J. Partezana, G. Sabol, B. Lai, Z. Cai, *J. ASTM Int.* **2005**, 2, 12375.
- [24] P. Barberis, T. Merle-Méjean, P. Quintard, *J. Nucl. Mater.* **1997**, 246, 232.
- [25] I. Idarraga, M. Mermoux, C. Duriez, A. Crisci, J. P. Mardon, *J. Nucl. Mater.* **2012**, 421, 160.
- [26] X. Zhao, D. Vanderbilt, *Phys. Rev. B* **2002**, 65, 075105.
- [27] M. Sternik, K. Parlinski, *J. Chem. Phys.* **2005**, 122, 064707.
- [28] A. Kuwabara, T. Tohei, T. Yamamoto, I. Tanaka, *Phys. Rev. B* **2005**, 71, 064301.
- [29] C. W. Li, H. L. Smith, T. Lan, J. L. Niedziela, J. A. Muñoz, J. B. Keith, L. Mauger, D. L. Abernathy, B. Fultz, *Phys. Rev. B* **2015**, 91, 144302.
- [30] G. Wang, G. Luo, Y. L. Soo, R. F. Sabirianov, H.-J. Lin, W.-N. Mei, F. Namavar, C. L. Cheung, *Phys. Chem. Chem. Phys.* **2011**, 13, 19517.
- [31] M. Cardona, M. L. W. Thewalt, *Rev. Mod. Phys.* **2005**, 77, 1173.

[32] A. Feinberg, C. H. Perry, *J. Phys. Chem. Solids* **1981**, 42, 513.

[33] A. Meldrum, L. A. Boatner, R. C. Ewing, *Phys. Rev. Lett.* **2001**, 88, 025503.

### **SUPPORTING INFORMATION**

Additional supporting information may be found online in the Supporting Information section at the end of the article.

**How to cite this article:** Ciszak C, Mermoux M, Gutierrez G, et al. Raman spectra analysis of ZrO<sub>2</sub> thermally grown on Zircaloy substrates irradiated with heavy ion: Effects of oxygen isotopic substitution. *J Raman Spectrosc.* 2019;50:425–435. <https://doi.org/10.1002/jrs.5513>